Received: 7 August 2020 | Revised: 6 January 2021 | Accepted: 18 January 2021

DOI: 10.1111/odi.13780

ORIGINAL ARTICLE

ORAL DISEASES WILEY

Age-related dental phenotypes and tooth characteristics of *FAM83H*-associated hypocalcified amelogenesis imperfecta

Kanokwan Sriwattanapong[1] | Issree Nitayavardhana[2] | Thanakorn Theerapanon[1] | Sermporn Thaweesapphithak[3] | Pintu-On Chantarawaratit[4] | Rakkierti Garuyakich[2] | Chureerat Phokaew[5,6] | Thantrira Porntaveetus[1,2] | Vorasuk Shotelersuk[5,6]

[1]Genomics and Precision Dentistry Research Unit, Department of Physiology, Faculty of Dentistry, Chulalongkorn University, Bangkok, Thailand

[2]Geriatric Dentistry and Special Patients Care Clinic, Faculty of Dentistry, Chulalongkorn University, Bangkok, Thailand

[3]Center of Excellence in Regenerative Dentistry, Faculty of Dentistry, Chulalongkorn University, Bangkok, Thailand

[4]Department of Orthodontics, Faculty of Dentistry, Chulalongkorn University, Bangkok, Thailand

[5]Center of Excellence for Medical Genomics, Medical Genomics Cluster, Department of Pediatrics, Faculty of Medicine, Chulalongkorn University, Bangkok, Thailand

[6]Excellence Center for Genomics and Precision Medicine, King Chulalongkorn Memorial Hospital, The Thai Red Cross Society, Bangkok, Thailand

Correspondence
Thantrira Porntaveetus, Genomics and Precision Dentistry Research Unit, Department of Physiology, Faculty of Dentistry, Chulalongkorn University, Bangkok 10330, Thailand.
Email: thantrira.p@chula.ac.th

Funding information
Faculty of Dentistry, Chulalongkorn University, Grant/Award Number: DRF64013; Thailand Research Fund, Grant/Award Number: RSA6280001 and DPG6180001; Global partnership, Grant/Award Number: CU-C16F630029; Thailand Science Research and Innovation, Grant/Award Number: CU_FRB640001_01_32_3 and CU_FRB640001_01_32_4; Chulalongkorn University; Health Systems Research Institute; National Research Council of Thailand

Abstract

Objectives: Autosomal-dominant hypocalcified amelogenesis imperfecta (ADHCAI) shows phenotypic heterogeneity. Our aim was to characterise the ADHCAI phenotypes, tooth properties and genotypes.

Methods: Three unrelated ADHCAI probands and seven additional affected members of the three families were recruited. Mutations were identified by exome and Sanger sequencing, and haplotypes by SNP array. Tooth colour, roughness, density, nanohardness, minerals and ultrastructure were investigated.

Results: Ten participants were heterozygous for the *FAM83H* mutation c.1387C>T (p.Gln463*). All shared a 3.43 Mbp region on chromosome 8q24.3 encompassing the *FAM83H* variant, indicating a common ancestry. The c.1387C>T was estimated to be 23.8 generations or 600 years. The *FAM83H* enamel had higher roughness and lower lightness, density, nanohardness, and calcium and phosphorus levels than controls. Blunted enamel rods, wide interrod spaces and disorganised dentinoenamel junctions were observed. Evaluating the patients with the same mutation and reviewing others with different mutations in *FAM83H* revealed that the *FAM83H* heterogeneous phenotypes are age-influenced. Tooth colour and surface texture change with ageing.

Conclusions: *FAM83H* enamel demonstrated decreased lightness, density, hardness, calcium, phosphorus and defective ultrastructure. We have identified that the phenotypic variation in *FAM83H*-associated ADHCAI is age-related. Awareness of the correlation between age and clinical features of *FAM83H*-ADHCAI can help dentists make an accurate diagnosis.

KEYWORDS

enamel, hypomineralisation, lightness, mineral density, nanohardness, roughness

1 | INTRODUCTION

Amelogenesis imperfecta (AI) is a phenotypically and genotypically heterogeneous group of enamel anomalies affecting the primary and permanent dentitions. The most common classification proposed by Witkop (1988) categorised AI based on phenotype into four types including hypoplastic, hypomaturation, hypocalcification and hypomaturation-hypoplastic with taurodontism and then subdivided into 15 subtypes based on phenotype and mode of inheritance (Witkop, 1988). To date, mutations in 28 genes have been associated with AI according to the Human Phenotype Ontology (HPO) (Köhler et al., 2018) and Leiden Open Variation Database (LOVD) v.3.0 (Fokkema et al., 2011). The genes mutated in AI are involved in amelogenesis with diverse functions such as the enamel matric proteins (*AMELX, ENAM and AMBN*), the enamel matric proteases (*MMP20 and KLK4*), cell–cell and cell–matrix adhesion (*FAM83H, ITGB6, LAMA3 and LAMB3*) and ion transport (*WDR72 and SLC24A4*) (Nitayavardhana et al., 2020; Smith et al., 2017).

The *FAM83H* gene (OMIM#130900) functions as the linker between casein kinase 1α and keratin (Fulcher et al., 2018; Kuga et al., 2016). It is highly expressed in the presecretory and secretory ameloblasts and plays an important role during enamel calcification (Kim et al., 2008). Mutations in *FAM83H* are associated with autosomal-dominant hypocalcified AI (ADHCAI; OMIM 130,900), which is the most prevalent and severe AI type (Crawford et al., 2007; Witkop, 1988). To date, fifty mutations in *FAM83H* have been reported (LOVD v3.0 and ClinVar) (Fokkema et al., 2011; Landrum et al., 2018). These mutations are exclusively found in the last exon, exon 5, and are truncating mutations, except for two missense variants. Although the type and location of mutations are specific, the *FAM83H*-ADHCAI phenotypes are diverse (Kim et al., 2008; Mendoza et al., 2007; Nowwarote et al., 2018; Wright et al., 2011). Currently, the phenotype–genotype correlation of *FAM83H* mutations has not been established, and the understanding of tooth properties related to *FAM83H*-ADHCAI is minimal.

This study aimed to thoroughly characterise the phenotype, genotype and tooth characteristics (physical, mechanical and ultrastructural features) associated with ADHCAI. Three Thai patients from 3 different families were recruited. Whole-exome sequencing identified that all three patients possessed the same nonsense mutation, c. 1387C>T, p.Gln463*, in *FAM83H*. From the 31 reportedly affected members in these three families, 10 patients were recruited for phenotypic and genotypic characterisation. Haplotype and relatedness analyses were performed. This study identified the patients sharing the same *FAM83H* mutation and evaluated their phenotypes compared with the patients in previous reports. We have found that the heterogeneous phenotypes of ADHCAI are age-related. In addition, the physical, mechanical and ultrastructural features of *FAM83H*-ADHCAI are revealed.

2 | MATERIALS AND METHODS

2.1 | Subjects

Three unrelated Thai patients affected with ADHCAI were recruited. Families 1, 2 and 3 were reported to have 9, 14 and 8 affected members, respectively. Of these 31 individuals, 10 were available for phenotypic and genotypic studies (Figure 1, Figure 2 and Figure S1). All participants or parents/guardians gave written informed consent for publication. Clinical and radiographic examinations were performed. The study was approved by the Research Ethics Committee (HREC-DCU 2017-078), Faculty of Dentistry, Chulalongkorn University and performed according to the ethical standards of the 1964 Declaration of Helsinki and its amendments.

2.2 | Whole-exome sequencing (WES) and Sanger sequencing

Genomic DNA was extracted from peripheral blood leucocytes. WES was performed using Illumina Hiseq4000 sequencer at Macrogen Inc. (Seoul, Korea) (Intarak et al., 2019; Porntaveetus et al., 2018). The variants were filtered following these criteria: (a) passed all quality filters during the variants calling process, (b) had a read depth > 10, (c) located in the coding regions and canonical splice sites of genes related to amelogenesis imperfecta (Smith et al., 2017), and (d) had < 1% minor allele frequency in the Genome Aggregation Database (gnomAD), Exome Variant Server, 1,000 Genomes Project Consortium, dbSNPs, and in-house database of 2,166 Thai exomes. Pathogenicity of the filtered variant was classified according to the ACMG standards and guidelines (Richards et al., 2015). The pathogenic variant was validated by Sanger sequencing using primers F: TTCTTCCAGGCGCGGCACCT and R: GAAGTCATCCGGGTCCGCGA.

2.3 | Single Nucleotide Polymorphism (SNP) array genotyping

SNP genotyping was achieved using the Infinium OmniZhongHua-8 BeadChip microarray containing 1,175,489 SNPs (Illumina, Seoul, South Korea). Ten participants including Family 1 (Patient 1, parents and grandmother), Family 2 (Patient 2, parents and aunt) and Family 3 (Patient 3 and daughter) were included for haplotype analysis. The SNPs genotype data from position 140,812,347 (rs12679196) to 146,301,427 (kgp22790488) in chromosome 8 that encompasses the *FAM83H* gene were extracted from whole SNP array data. The SNPs that were missing in any individuals were excluded. The genotype data from each family were then phased to define the ancestral haplotypes that linked with

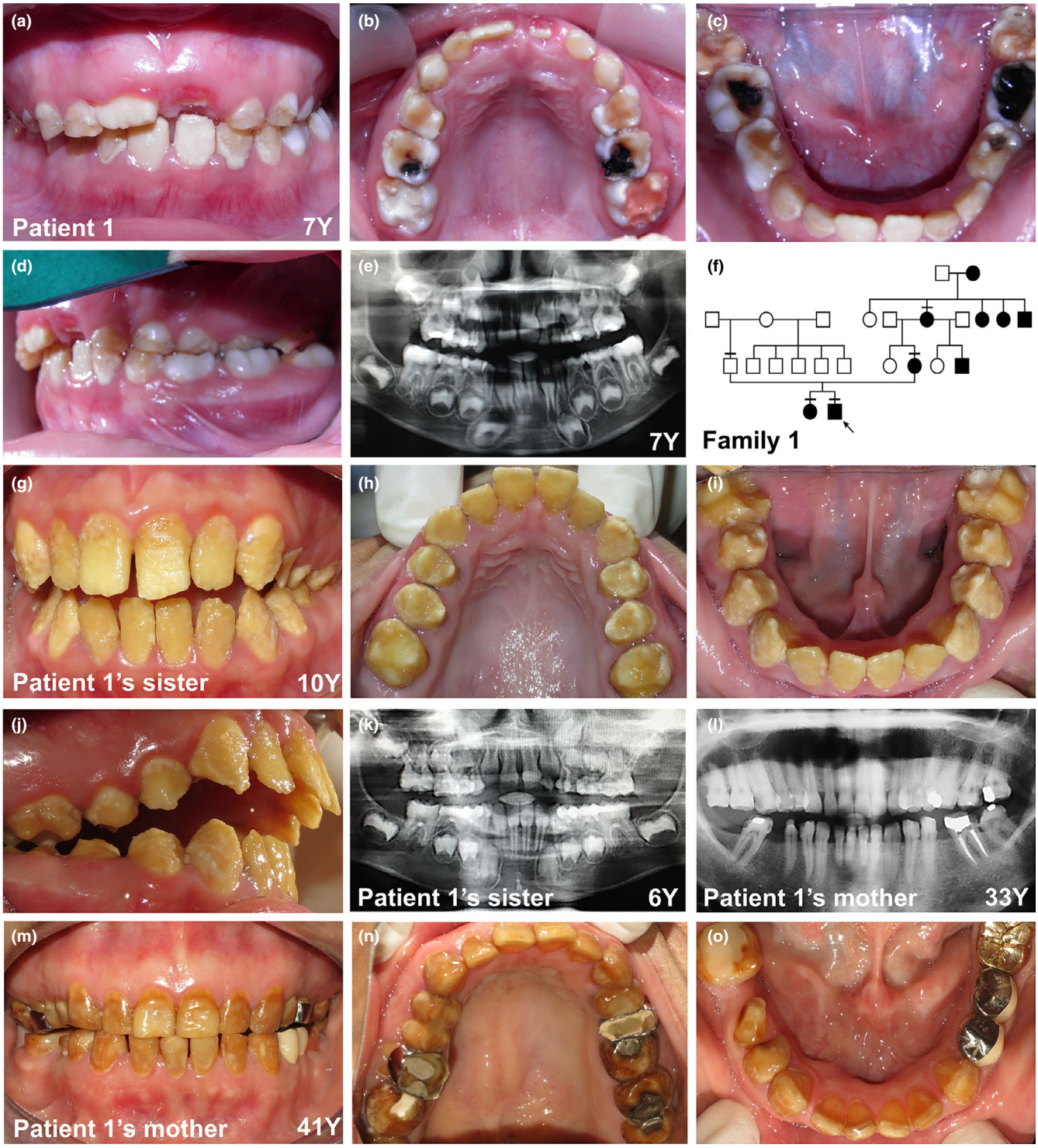

FIGURE 1 Phenotypes and pedigree of Family 1. (a–d) Clinical images of Patient 1 at age 7 years show porous and yellowish teeth. Normal-looking enamel was present on the buccal and lingual surfaces and cusp tips of primary molars and first molars. (e) Panoramic radiograph demonstrated enamel loss on the erupted teeth, normal thickness of enamel on the unerupted teeth, and reduced radiodensity contrast between enamel and dentine. (f) Pedigree of Family1. Males are marked by squares and females by circles. Filled symbols indicate reportedly affected individuals. An arrow indicates the proband. A horizontal line above symbol indicates an individual having Sanger sequencing. (g–j) Clinical image of Patient 1's sister at 10 years of age exhibited cheesy-soft teeth and anterior open bite. (k) Panoramic radiograph of Patient 1's sister at 6 years of age showed that the erupted teeth had reduced enamel thickness and radiopacity. (l–o) Patient 1's mother had brown and glossy teeth with scattered small white patches. The lower left second molar was endodontically treated. The lower first molars were previously extracted. The panoramic radiograph showed thin enamel with reduced radiodensity. Y, years of age

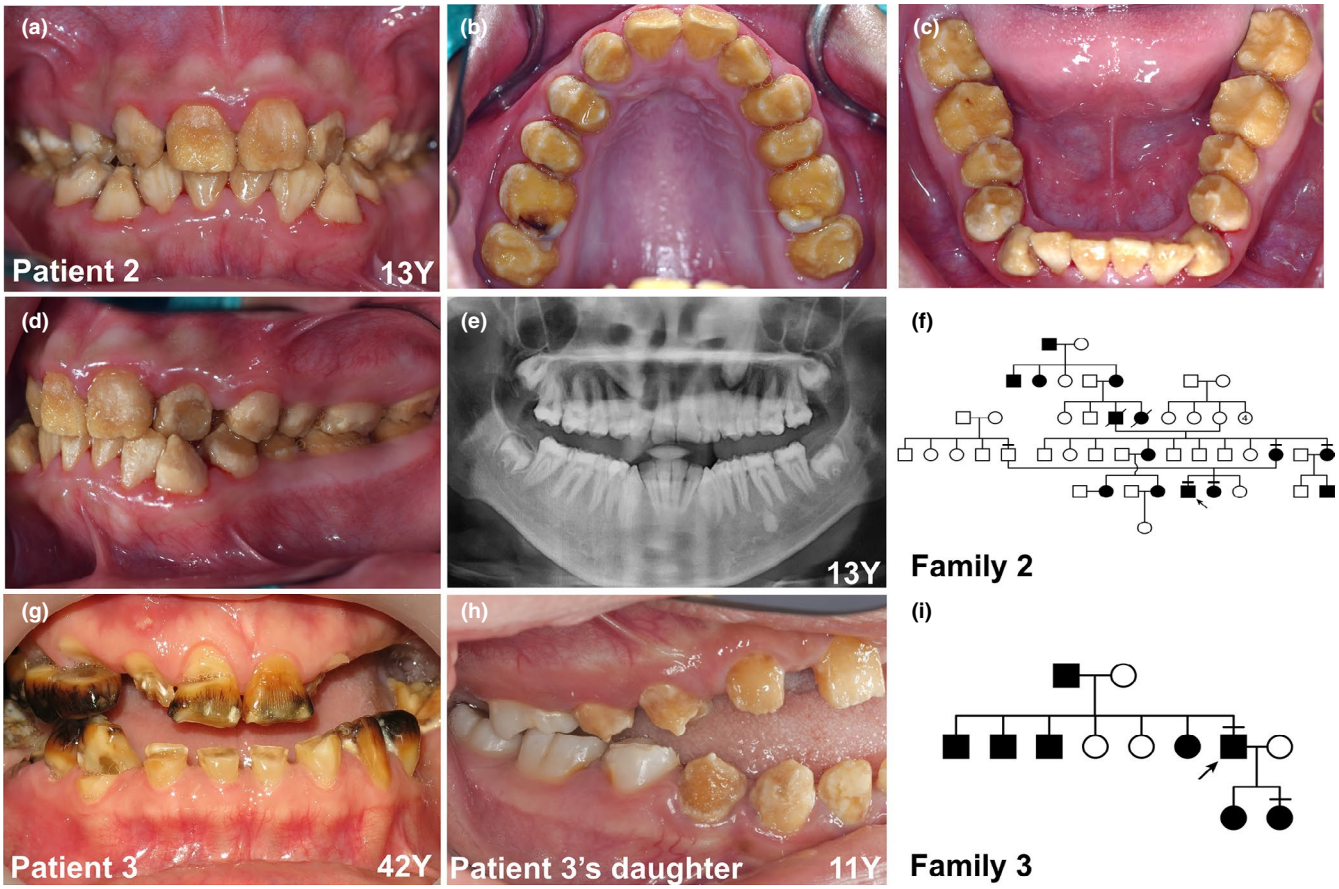

FIGURE 2 Phenotypes and pedigree of Families 2 and 3. (a–e) Clinical and radiographic images of Patient 2 at 13 years of age showed yellowish, discoloured, rough and soft teeth. Panoramic radiograph presented reduced contrast between the enamel and dentine and embedded maxillary canines. The erupted teeth had minimal enamel thickness. (f) Pedigree of Family 2. Males are marked by squares and females by circles. Filled symbols indicate reportedly affected individuals. An arrow indicates the proband. A horizontal line above symbol indicates an individual having Sanger sequencing. (g) Patient 3 at age 42 years had smooth, shiny, brownish-black teeth (h) Patient 3's daughter presented rough and yellow teeth. Normal-looking enamel was present on the buccal and lingual surfaces of the posterior teeth. (i) Pedigree of Family 3. Males are marked by squares and females by circles. Filled symbols indicate reportedly affected individuals. An arrow indicates the proband. A horizontal line above symbol indicates an individual having Sanger sequencing

the mutation. The coordinates of the shared ancestral segments from each family were input into the Genetic Mutation Age Estimator program (https://shiny.wehi.edu.au/rafehi.h/mutation-dating) to estimate the mutation's age (Gandolfo et al., 2014; Yeetong et al., 2019).

2.4 | Tooth samples analyses

A primary upper left lateral incisor (AI1), permanent lower right first premolar (AI2) and permanent upper right lateral incisor (AI3) were collected from Patients 1, 2 and 3, respectively. Each AI sample was evaluated in comparison with three tooth type-matched controls collected from age-matched healthy individuals. For AI3, only the root portion was available for evaluation.

Tooth colour was measured on the buccal and lingual surfaces (3 times/surface) using a digital spectrophotometer (VITA Easyshade® V, Bad Sackingen, Germany) based on the CIE L*a*b* colour scale of the International Commission on Illumination.

Mineral density was evaluated by a micro-computerised tomographic machine (μCT35, Scanco Medical, Brüttisellen, Switzerland). Thirty layers of enamel and dentine were selected. The images were processed using Image Processing Language (Scanco Medical AG, Wangen-Brüttisellen, Switzerland).

The tooth surface roughness was measured as surface topography parameter by the Talyscan 150 and the TalyMap Universal program (Taylor Hobson Ltd, Leicester, United Kingdom). Thirty spots every 600 μm were selected.

Nanohardness were measured on longitudinal sections of the samples (30 locations) using a nano-base indentation system (Ultra Micro-Indentation System, UMIS II, CSIRO, Canberra, Australia).

The sections were dried using a critical point dryer (Emitech K850, Emitech Ltd, Kent, England) and covered with gold powder (JFC 1200, Tokyo, Japan). The elemental levels (%) of carbon (C), oxygen (O), phosphorus (P) and calcium (Ca) were measured at 3 locations using EDX (ISIS 300 EDX-system; Oxford Instruments, UK). Tooth ultrastructure was examined by an SEM (Quanta Feg 250, FEI Company, Oregon, USA).

Comparisons between the ADHCAI and control teeth were determined using the independent *t* test ($p < .05$) (GraphPad Prism5 Software Inc., San Diego, CA, USA).

3 | RESULTS

3.1 | Clinical manifestations of ADHCAI

Patient 1, a 7-year-old boy, presented with tooth sensitivity. His oral examination revealed that the patient had porous and yellowish teeth with an extensive loss of enamel and exposed dentine. The remaining white and chalky enamel was observed on the buccal and lingual surfaces and cusp tips of the deciduous molars and permanent first molars. The erupting permanent incisors' enamel was mildly yellowish and porous. The panoramic radiograph showed reduced radiodensity contrast between the enamel and dentine, thin enamel on the erupted teeth, and normal enamel thickness on the unerupted teeth (Figure 1a–e). A primary upper left lateral incisor was extracted due to prolonged retention (AI1 sample). Anterior open bite was not present. The patient's sister (10 years old) exhibited cheesy-soft teeth. The enamel was partially lost, exposing yellowish dentine. Normal-looking enamel was present along the gingival margins and cusp tips of the teeth. Anterior open bite was present (Figure 1g–k). Patient 1's mother, aged 41 years, exhibited yellow to brownish discoloured teeth. Severe enamel loss was present, leaving shiny brown dentine with scattered small white patches. Both lower first molars were extracted due to irreversible pulpitis, and the lower left second molar was endodontically treated. The panoramic radiograph showed thin enamel with reduced radiodensity (Figure 1l–o). The family pedigree of Patient 1 showed 9 affected family members (Figure 1f).

Patient 2, a 13-year-old boy, complained of yellow and sensitive teeth. His oral examination revealed generalised tooth discolouration with irregular texture, anterior tooth crowding and crossbite. Normal-looking enamel was present along the cervical areas and cusp tips of the teeth (Figure 2a–d). The radiograph exhibited embedded upper canines. The unerupted third molars had a normal enamel thickness, while the erupted teeth had thin enamel with reduced radiopacity (Figure 2e). The lower right first premolar (AI2 sample) was extracted according to the orthodontic treatment plan. The family pedigree of Patient 2 revealed an AI phenotype in five generations (Figure 2f).

Patient 3, a 42-year-old male, presented with smooth, shiny, brownish-black teeth with severe wear, dental caries and multiple retained roots. The clinical and radiographic features of this family were previously reported (Kantaputra et al., 2016). The upper left lateral incisor (AI3 sample) was extracted. Patient 3's daughter had soft, porous and yellowish teeth. Normal-appearing enamel was observed on the buccal and lingual surfaces of the posterior teeth. Anterior open bite was present (Figure 2h).

We found that all affected patients had generalised plaque accumulation, gingival inflammation and multiple dental cavities. The medical history of the three families revealed no significant systemic diseases or medications affecting the teeth.

3.2 | Mutation analyses

WES identified that Patients 1, 2 and 3 harboured the same heterozygous nonsense mutation, c.1387C>T, p.Gln463*, in the exon 5 of *FAM83H* (NM_198488.5). The variant was classified as pathogenic based on the ACMG standards and guidelines (PVS1, PM2, PP1 and PP3) (Richards et al., 2015). Sanger sequencing confirmed the presence of the mutation in the patients and all available affected family members (Figure S1). The inheritance pattern, genetic mutation and phenotypic features found in these three families indicated ADHCAI.

3.3 | SNP array genotyping

Because the three families with the same ethnicity possessed the same *FAM83H* mutation, it was speculated that they might have a common ancestry. We first performed haplotype analysis in the family with the largest number of affected members, Family 2 (Patient 2, parents and aunt), and detected a 3.41 Mbp segment between coordinates 142,883,316 and 146,293,414 on chromosome 8q24.3 segregating in the affected members. Next, we analysed the affected members in Family 3 (Patient 3 and his daughter) and Family 1 (Patient 1, parents, and grandmother) and detected a common 3.43 Mbp segment between coordinates 142,862,278 and 146,293,414. This region covered the shared 3.41 Mbp segment identified in Family 2 and the c.1387C>T variant in *FAM83H*.

The coordinates were input into the Genetic Mutation Age Estimator program (https://shiny.wehi.edu.au/rafehi.h/mutation-dating) (Gandolfo et al., 2014; Yeetong et al., 2019). It was estimated that the age of c.1387C>T variant was 23.8 generations or 600 years (assuming one generation = 25 years) with a 95% confidence interval (CI) between 7.4 (175 years) and 84.3 (2,100 years) generations. These estimations suggest that the c.1387C>T mutation is identical by descent and these three families have a common ancestry.

3.4 | Characteristics of the deciduous and permanent teeth affected with *FAM83H*-ADHCAI

The exfoliated deciduous upper left lateral incisor (AI1) was collected from Patient 1. The permanent lower right first premolar (AI2) in Patient 2 was extracted according to orthodontic treatment plan. The retained root of the permanent upper right lateral incisor (AI3) in Patient 3 was extracted due to non-restorable condition. All patients donated the tooth samples for this study. We examined the physical, mechanical and ultrastructural features of the AI teeth compared with controls.

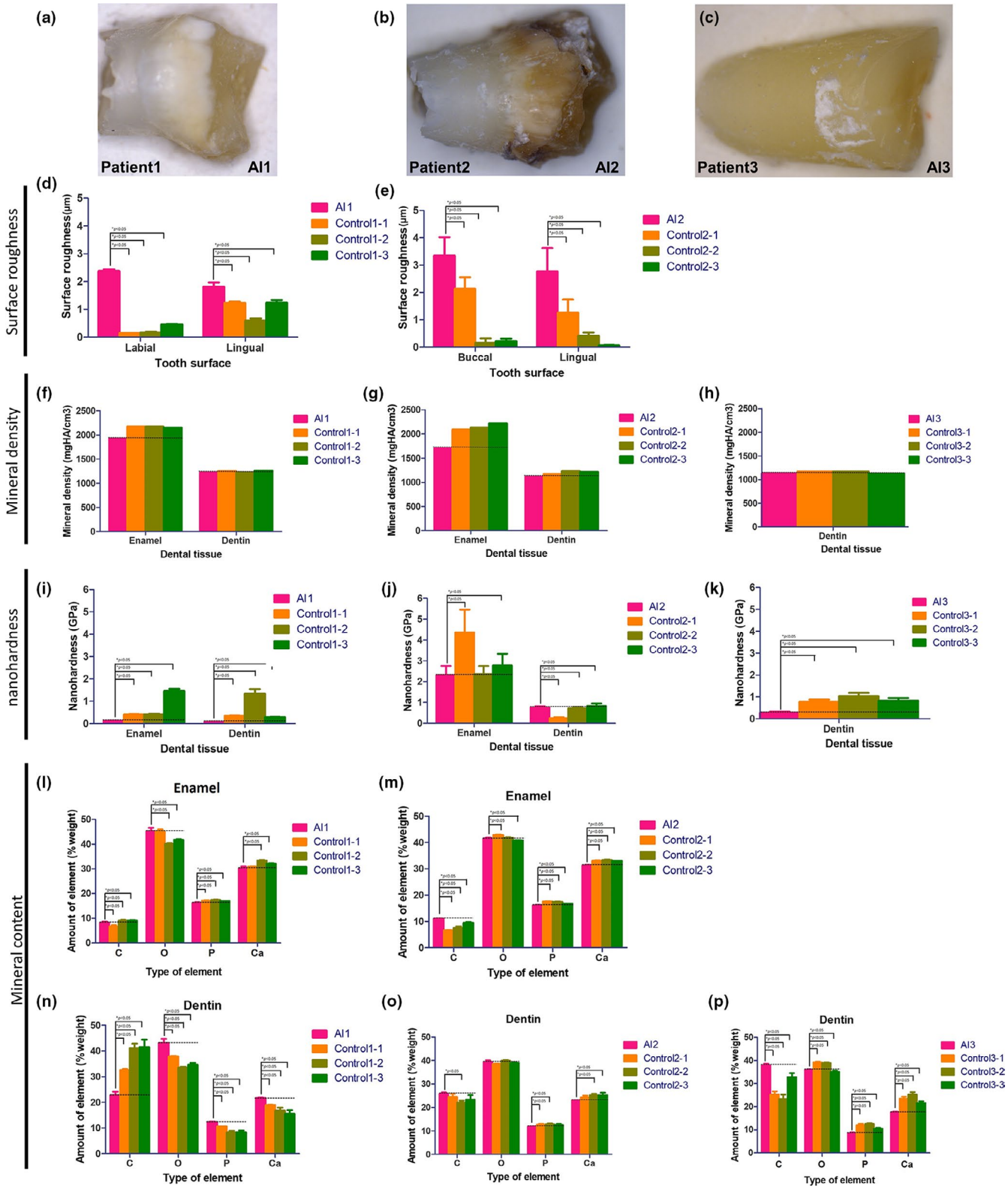

FIGURE 3 Tooth characteristics and phenotypic properties. (a) Microscopic images of the primary upper left lateral incisor (AI1) obtained from Patient1 had yellow and opaque white enamel and exposed dentine. (b) The permanent lower right first premolar (AI2) obtained from Patient 2 was dark yellow in colour and had an irregular surface. (c) The permanent upper right lateral incisor (AI3) obtained from Patient 3 had a smooth and yellow root. (d, e) The surface roughness values of AI1 and AI2 were significantly higher than those of controls ($p < .05$). (f–h) The mineral density differences in enamel and dentine between patients and controls were not statistically significant. (i–k) Nanohardness values of AI1 and AI2 enamel were significantly decreased compared to control values. In dentine, AI1 and AI3 showed lower nanohardness values than controls ($p < .05$). (l–m) AI1 and AI2 enamel demonstrated siginificantly lower Ca and P levels than controls. (n–p) AI2 and AI3 dentine revealed significantly lower Ca and P levels than controls whereas AI1 had significantly higher Ca and P than controls. C, carbon; O, oxygen; P, phosphorus; Ca, calcium

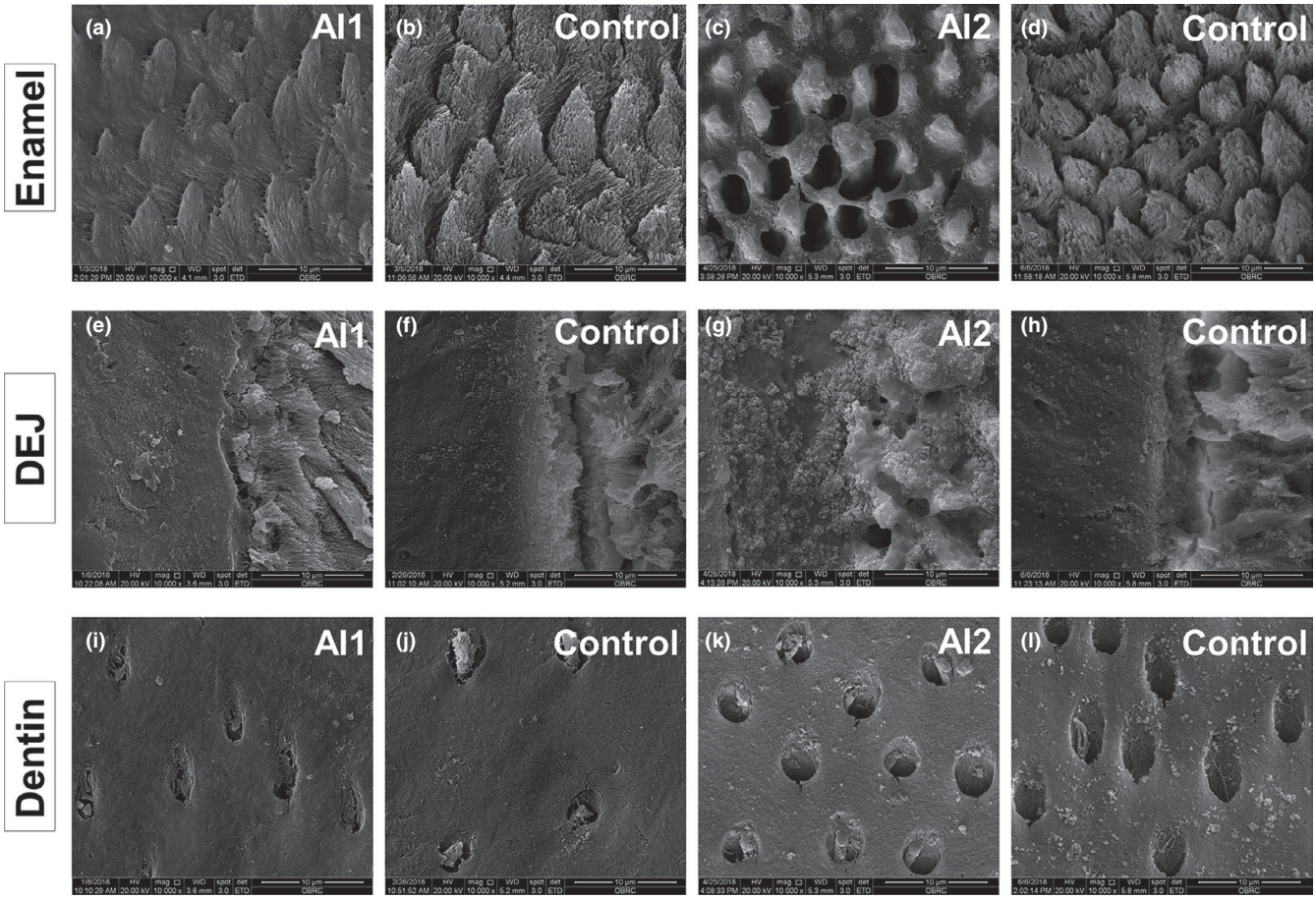

FIGURE 4 Tooth ultrastructure. (a–d) Scanning electron microscopic images of the AI1 and AI2 enamel had rounded and short enamel rods with wider interrod areas compared with control. Porosities were seen in the AI2 enamel. (e–h) Disorganised dentinoenamel junctions (DEJ) were present in AI1 and AI2. (i–l) The dentine ultrastructure and dentinal tubules of AI1 and AI2 were comparable to controls. SEM images at 10,000× magnification

3.5 | Gross characteristics

AI1 had yellowish and rough enamel with white patches (Figure 3a). AI2 had yellow-brown and rough enamel with demineralised spots and AI3 had yellow and smooth root surface (Figure 3a–c). Based on the CIE LAB, the crown portions of AI1 and AI2 were darker, redder and yellower compared with controls. Similarly, the root portions of AI1, AI2 and AI3 were darker and redder compared with controls. The colour differences between the AI teeth and controls were perceivable by the human eye ($\Delta E > 2$) (Tables S1 and S2). The surface roughness values of the AI1 and AI2 crowns were significantly greater than those of controls (Figure 3d–e).

3.6 | Ultrastructural characteristics

Micro-CT revealed that the differences in the enamel and dentine mineral density between patients and controls were not statistically significant (Figure 3f–h, Tables S3 and S4). Mechanical property evaluation indicated that the nanohardness values of the AI1 and AI2 enamel and of the AI1 and AI3 dentine were significantly lower than those of controls (Figure 3i–k). EDX demonstrated that the AI1 and AI2 enamel had significantly reduced phosphorus and calcium content compared with controls. In dentine, the AI2 and AI3 calcium and phosphorus levels were significantly lower, while those of AI1 were significantly higher, than those of controls (Figure 3l–p, Table S5).

SEM revealed that AI1 and AI2 had shorter and rounder enamel rods and wider interprismatic areas than controls. AI2 demonstrated severely disturbed enamel containing several holes. AI1 and AI2 showed disorganised dentinoenamel junctions (DEJ), while the controls had a continuous interface between the enamel and dentine. The dentine and dentinal tubules of the AI samples were comparable to controls (Figure 4).

3.7 | Phenotypic analysis of *FAM83H*-ADHCAI

Although our patients had the same *FAM83H* mutation, a wide range of clinical features were observed. We thoroughly characterised the phenotypes of our patients and those having different *FAM83H* mutations in previous reports (Chan et al., 2011;

Ding et al., 2009; El-Sayed et al., 2010; Gjørup et al., 2009; Hart et al., 2009; Haubek et al., 2011; Hyun et al., 2009; Kantaputra et al., 2016; Kim et al., 2008; Lee et al., 2008, 2011; Nowwarote et al., 2019; Nowwarote et al., 2018; Pourhashemi et al., 2014; Song et al., 2012; Urzua et al., 2015; Wang et al., 2020; Wright et al., 2009, 2011; Xin et al., 2017; Yu et al., 2018; Zhang et al., 2015; Zheng et al., 2020) (Table S6). We observed that the phenotypic differences in *FAM83H*-ADHCAI were age-related. Newly erupted permanent teeth are porous, soft, opaque white and slightly yellow. In the mixed dentition, the enamel gradually chips off. The teeth are still porous; however, the tooth colour becomes darker, likely due to accumulated food staining. Normal-looking enamel is seen at the cervical margins of the tooth crown and cusp tips. In adulthood, the teeth turn dark brown to black in colour and the tooth surfaces become smooth and shiny rather than soft and porous. It is expected that the exposed dentine is abraded and discoloration gradually increases over time (Figure 5).

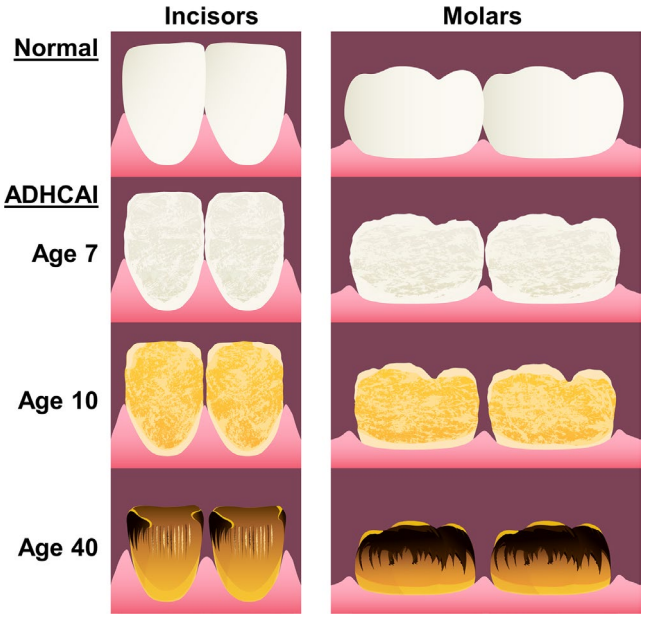

FIGURE 5 Clinical phenotypes of ADHCAI caused by *FAM83H* mutation

4 | DISCUSSION

The present study identified the ADHCAI patients caused by the nonsense mutation, c.1387C>T, p.Gln463*, in the exon 5 of *FAM83H*. The *FAM83H* gene consists of 5 exons. Exon 5 is the largest and contains all phosphorylation sites of the FAM83H protein. The C-terminus of the FAM83H protein contains evolutionarily conserved regions critical for amelogenesis (Huang et al., 2017). Among the genes causing AI, mutations in *FAM83H* are the most commonly found and produce the most severe enamel defects. The p.Gln463* mutation identified here is expected to generate a prematurely truncated FAM83H protein (NP_940890.4) lacking 717 amino acids. Consistent with previous studies, the ADHCAI-causing *FAM83H* mutations occur exclusively in the last exon and most mutations are truncating (LOVD v3.0 and ClinVar) (Fokkema et al., 2011; Landrum et al., 2018). *FAM83H* truncated mutations alter its subcellular localisation and act by a neomorphic mechanism to cause ADHCAI (Lee et al., 2011; Wang et al., 2019).

Although up to 50 pathogenic mutations in *FAM83H* have been reported, the c.1387C>T (p.Gln463*) mutation has been detected in only three families in Thailand. Haplotype analysis revealed that these 3 families shared a common 3.43 Mbp segment covering the *FAM83H* locus. These findings suggest that they have a common ancestor and the c.1387C>T mutation is identical by descent. It was estimated that the age of the c.1387C>T mutation was 23.8 generations or 600 years (assuming one generation = 25 years), with a 95% confidence interval (CI) between 7.4 (175 years) and 84.3 (2,100 years) generations. Similarly, a previous study found that the c.1366C>T mutation in *FAM83H* found in 5 Turkish families was identical by descent. This mutation was inherited from a common ancestor with a shared 1.8 Mb haplotype spanning the *FAM83H* locus (Hart et al., 2009). We show here that detection of identity by descent can be useful to estimate familial relatedness and fine-scale population structure (Browning & Browning, 2012).

Clinically, the *FAM83H*-ADHCAI teeth are generally rough and yellowish. In patients with *FAM83H* mutations, the quantity of enamel matrix proteins is normal; however, enamel calcification is disturbed (Hyun et al., 2009). Radiologically, the hypomineralised enamel appears to be of normal thickness, but has reduced contrast with dentine. After eruption, the enamel rapidly deteriorates, resulting in exposed dentine, loose proximal contacts and malocclusion. The tooth cervical regions and cusp tips are less affected by the mutation. Tooth sensitivity and infection are common problems of these patients. Other dental abnormalities reported in *FAM83H* patients include anterior open bite, embedded teeth, crowding and crossbite. In this study, anterior open bite was observed in 2 participants (Patient 1's sister and Patient 3's daughter). Moreover, an impacted canine and crossbite were found in Patient 2, similar to the patient reported by Xin et al., 2017 (Xin et al., 2017).

Phenotypic characterisation of the patients with the same mutation, c.1387C>T, p.Gln463*, in *FAM83H* reveals that the phenotypic differences in *FAM83H*-ADHCAI are age-related. Newly erupted teeth are porous, soft and slightly yellow. In young adults, the teeth are still porous, but darker in colour. The enamel is eroded leaving normal-looking enamel along the cervical margin of the tooth crown and cusp tips (Hart et al., 2009; Haubek et al., 2011; Nowwarote et al., 2019; Nowwarote et al., 2018; Song et al., 2012; Xin et al., 2017; Yu et al., 2018; Zhang et al., 2015). In adulthood, the teeth turn dark brown or black and the tooth surfaces become smooth and shiny rather than soft and porous. Most of the severely hypocalcified enamel in *FAM83H* teeth is usually worn down soon after the teeth erupt. However, the cusp tips on the premolars and molars and the areas along the gingival margin of the enamel are maintained for years and resist posteruptive enamel loss (Haubek et al., 2011; Lee et al., 2008). It is

suggested that the enamel on different tooth locations is differentially affected by the *FAM83H* mutation (Kantaputra et al., 2016). Following enamel loss, the exposed dark dentin could gradually trap external stain, leading to brown and black discoloured teeth in affected adults. The reasons of these changes can probably be due to the poor mineralisation degree of the enamel and other factors such as poor access to dental care, extrinsic pigmentation, medication, trauma and poor oral hygiene.

The *FAM83H* mutation reduces the enamel's physical and mechanical properties. The deciduous and permanent teeth with the *FAM83H* mutation had significantly increased surface roughness. Moreover, mineral density, nanohardness, and major inorganic substance levels, calcium and phosphorus, in *FAM83H* enamel were significantly less compared with controls. Ultrastructural analyses revealed that the *FAM83H* teeth had poorly formed enamel prisms and widened interrod spaces, consistent with previous reports (El-Sayed et al., 2010; Yu et al., 2018; Zhang et al., 2015). Unlike other studies, several holes were evident in the A12 enamel. These findings indicate that the enamel is dramatically disturbed during amelogenesis due to the *FAM83H* mutation (Kim et al., 2008; Wright et al., 2009). The relationship between low enamel hardness and increased tooth susceptibility to caries and fracture have been shown (Gutiérrez-Salazar & Reyes-Gasga, 2001). Enamel roughness also contributes to plaque and stain accumulation and dental caries initiation. These results suggest that the accumulated enamel defects in *FAM83H* teeth make them prone to rapid deterioration and dental diseases.

Sequential and reciprocal interactions between epithelial and mesenchymal tissues are essential mechanisms regulating the formation of enamel and dentine during tooth development (Thesleff, 2003). An integration between the enamel and dentin mineral is established via the regulation of mineral formation and organisation of the dentine and enamel matrices at the DEJ (Fang et al., 2011). We observed that the DEJ in *FAM83H* teeth was disorganised containing amorphous material. In dentine, the AI2 and AI3 calcium and phosphorus levels were significantly lower, while those of AI1 were significantly higher compared with controls. A previous study showed that the *FAM83H* tooth dentine exhibited irregular dentinal tubules with partly obliterated lumens and had less tubules, compared with those in normal controls (Zhang et al., 2015). Interglobular dentin representing incompletely calcified dentine matrix was also observed in some affected teeth (Wright et al., 2009). It was proposed that the *FAM83H* mutations not only disturbed enamel mineralisation, but also affected dentine formation (Zhang et al., 2015). Based on these findings, the *FAM83H* tooth dentine could be different from that of normal teeth.

To conclude, here, we identify the nonsense mutation, c.1387C>T (p.Gln463*), in *FAM83H* causing ADHCAI in the patients sharing a common ancestor. *FAM83H*-ADHCAI exhibits deteriorated tooth ultrastructural, physical and mechanical characteristics. We also demonstrate that the heterogeneous clinical features of *FAM83H*-ADHCAI are age-related. These findings broaden the understanding of the phenotypic spectrum of *FAM83H*-ADHCAI leading to prompt prognosis and dental management for ADHCAI patients.

ACKNOWLEDGEMENTS

This project is funded by the National Research Council of Thailand, TSRI Fund (CU_FRB640001_01_32_3, CU_FRB640001_01_32_4), Global partnership CU-C16F630029, Health Systems Research Institute, Thailand Research Fund (MRG6280001, DPG6180001), and Faculty Research Grant (DRF64013), Faculty of Dentistry, Chulalongkorn University. KS is supported by the Ratchadapisek Somphot Fund for Postdoctoral Fellowship, Chulalongkorn University. ST is supported by the 100th Anniversary Chulalongkorn University Fund for Doctoral Scholarship and the 90th Anniversary of Chulalongkorn University Fund (Ratchadaphiseksomphot Endowment Fund). We thank Dr. Kevin A. Tompkins for language revision of the manuscript.

CONFLICT OF INTEREST

The authors declare no competing interests.

AUTHOR CONTRIBUTIONS

Kanokwan Sriwattanapong: Data curation; investigation; writing–original draft; writing–review and editing. **Issree Nitayavardhana:** Investigation; writing–review and editing. **Thanakorn Theerapanon:** Investigation; writing–review and editing. **Sermporn Thaweesapphithak:** Investigation; writing–review and editing. **Pintu-On Chantarawaratit:** Investigation; writing–review and editing. **Rakkierti Garuyakich:** Investigation; writing–review and editing. **Chureerat Phokaew:** Data curation; writing–review and editing. **Thantrira Porntaveetus:** Conceptualization; formal analysis; writing–original draft; writing–review and editing. **Vorasuk Shotelersuk:** Formal analysis; resources; writing–review and editing.

PEER REVIEW

The peer review history for this article is available at https://publons.com/publon/10.1111/odi.13780.

ORCID

Thanakorn Theerapanon https://orcid.org/0000-0001-6727-862X
Thantrira Porntaveetus https://orcid.org/0000-0003-0145-9801

REFERENCES

Browning, S. R., & Browning, B. L. (2012). Identity by descent between distant relatives: Detection and applications. *Annual Review of Genetics*, *46*(1), 617–633. https://doi.org/10.1146/annurev-genet-110711-155534

Chan, H. C., Estrella, N. M., Milkovich, R. N., Kim, J. W., Simmer, J. P., & Hu, J. C. (2011). Target gene analyses of 39 amelogenesis imperfecta kindreds. *European Journal of Oral Sciences*, *119*(Suppl 1), 311–323. https://doi.org/10.1111/j.1600-0722.2011.00857.x

Crawford, P. J., Aldred, M., & Bloch-Zupan, A. (2007). Amelogenesis imperfecta. *Orphanet Journal of Rare Diseases*, *2*, 17. https://doi.org/10.1186/1750-1172-2-17

Ding, Y., Estrella, M., Hu, Y. Y., Chan, H. L., Zhang, H. D., Kim, J.-W., Simmer, J. P., & Hu, J.-C. (2009). Fam83h is associated with intracellular vesicles and ADHCAI. *Journal of Dental Research*, *88*(11), 991–996. https://doi.org/10.1177/0022034509349454

El-Sayed, W., Shore, R. C., Parry, D. A., Inglehearn, C. F., & Mighell, A. J. (2010). Ultrastructural analyses of deciduous teeth affected by hypocalcified amelogenesis imperfecta from a family with a novel Y458X FAM83H nonsense mutation. *Cells Tissues Organs*, *191*(3), 235–239. https://doi.org/10.1159/000252801

Fang, P.-A., Lam, R. S. K., & Beniash, E. (2011). Relationships between dentin and enamel mineral at the dentino-enamel boundary: Electron tomography and high-resolution transmission electron microscopy study. *European Journal of Oral Sciences*, *119*(Suppl 1), 120–124. https://doi.org/10.1111/j.1600-0722.2011.00876.x

Fokkema, I. F. A. C., Taschner, P. E. M., Schaafsma, G. C. P., Celli, J., Laros, J. F. J., & den Dunnen, J. T. (2011). LOVD vol 2.0: The next generation in gene variant databases. *Human Mutation*, *32*(5), 557–563. https://doi.org/10.1002/humu.21438

Fulcher, L. J., Bozatzi, P., Tachie-Menson, T., Wu, K. Z. L., Cummins, T. D., Bufton, J. C., Pinkas, D. M., Dunbar, K., Shrestha, S., Wood, N. T., Weidlich, S., Macartney, T. J., Varghese, J., Gourlay, R., Campbell, D. G., Dingwell, K. S., Smith, J. C., Bullock, A. N., & Sapkota, G. P. (2018). The DUF1669 domain of FAM83 family proteins anchor casein kinase 1 isoforms. *Science Signaling*, *11*(531), eaao2341. https://doi.org/10.1126/scisignal.aao2341

Gandolfo, L. C., Bahlo, M., & Speed, T. P. (2014). Dating rare mutations from small samples with dense marker data. *Genetics*, *197*(4), 1315–1327. https://doi.org/10.1534/genetics.114.164616

Gjørup, H., Haubek, D., Hintze, H., Haukali, G., Løvschall, H., Hertz, J. M., & Poulsen, S. (2009). Hypocalcified type of amelogenesis imperfecta in a large family: Clinical, radiographic, and histological findings, associated dento-facial anomalies, and resulting treatment load. *Acta Odontologica Scandinavica*, *67*(4), 240–247. https://doi.org/10.1080/00016350902973685

Gutiérrez-Salazar, M., & Reyes-Gasga, J. (2001). Enamel hardness and caries susceptibility in human teeth. *Revista Latinoamericana De Metalurgia Y Materiales*, *21*, 36–40.

Hart, P. S., Becerik, S., Cogulu, D., Emingil, G., Ozdemir-Ozenen, D., Han, S. T., & Hart, T. C. (2009). Novel FAM83H mutations in Turkish families with autosomal dominant hypocalcified amelogenesis imperfecta. *Clinical Genetics*, *75*(4), 401–404. https://doi.org/10.1111/j.1399-0004.2008.01112.x

Haubek, D., Gjørup, H., Jensen, L. G., Juncker, I., Nyegaard, M., Børglum, A. D., Poulsen, S., & Hertz, J. M. (2011). Limited phenotypic variation of hypocalcified amelogenesis imperfecta in a Danish five-generation family with a novel FAM83H nonsense mutation. *International Journal of Paediatric Dentistry*, *21*(6), 407–412. https://doi.org/10.1111/j.1365-263X.2011.01142.x

Huang, W., Yang, M., Wang, C., & Song, Y. (2017). Evolutionary analysis of FAM83H in vertebrates. *PLoS One*, *12*(7), e0180360. https://doi.org/10.1371/journal.pone.0180360

Hyun, H. K., Lee, S. K., Lee, K. E., Kang, H. Y., Kim, E. J., Choung, P. H., & Kim, J. W. (2009). Identification of a novel FAM83H mutation and microhardness of an affected molar in autosomal dominant hypocalcified amelogenesis imperfecta. *International Endodontic Journal*, *42*(11), 1039–1043. https://doi.org/10.1111/j.1365-2591.2009.01617.x

Intarak, N., Theerapanon, T., Thaweesapphithak, S., Suphapeetiporn, K., Porntaveetus, T., & Shotelersuk, V. (2019). Genotype-phenotype correlation and expansion of orodental anomalies in LTBP3-related disorders. *Molecular Genetics and Genomics*, *294*(3), 773–787. https://doi.org/10.1007/s00438-019-01547-x

Kantaputra, P. N., Intachai, W., & Auychai, P. (2016). All enamel is not created equal: Supports from a novel FAM83H mutation. *American Jounral of Medical Genetics Part A*, *170a*(1), 273–276. https://doi.org/10.1002/ajmg.a.37406

Kim, J.-W., Lee, S.-K., Lee, Z. H., Park, J.-C., Lee, K.-E., Lee, M.-H., Park, J.-T., Seo, B.-M., Hu, J.-C., & Simmer, J. P. (2008). FAM83H mutations in families with autosomal-dominant hypocalcified amelogenesis imperfecta. *American Jounal of Human Genetics*, *82*(2), 489–494. https://doi.org/10.1016/j.ajhg.2007.09.020

Köhler, S., Carmody, L., Vasilevsky, N., Jacobsen, J. O. B., Danis, D., Gourdine, J.-P., Gargano, M., Harris, N. L., Matentzoglu, N., McMurry, J. A., Osumi-Sutherland, D., Cipriani, V., Balhoff, J. P., Conlin, T., Blau, H., Baynam, G., Palmer, R., Gratian, D., Dawkins, H., … Robinson, P. N. (2018). Expansion of the Human Phenotype Ontology (HPO) knowledge base and resources. *Nucleic Acids Research*, *47*(D1), D1018–D1027. https://doi.org/10.1093/nar/gky1105

Kuga, T., Kume, H., Adachi, J., Kawasaki, N., Shimizu, M., Hoshino, I., Matsubara, H., Saito, Y., Nakayama, Y., & Tomonaga, T. (2016). Casein kinase 1 is recruited to nuclear speckles by FAM83H and SON. *Scientific Reports*, *6*, 34472. https://doi.org/10.1038/srep34472

Landrum, M. J., Lee, J. M., Benson, M., Brown, G. R., Chao, C., Chitipiralla, S., Gu, B., Hart, J., Hoffman, D., Jang, W., Karapetyan, K., Katz, K., Liu, C., Maddipatla, Z., Malheiro, A., McDaniel, K., Ovetsky, M., Riley, G., Zhou, G., … Maglott, D. R. (2018). ClinVar: Improving access to variant interpretations and supporting evidence. *Nucleic Acids Research*, *46*(D1), D1062–d1067. https://doi.org/10.1093/nar/gkx1153

Lee, S. K., Hu, J. C., Bartlett, J. D., Lee, K. E., Lin, B. P., Simmer, J. P., & Kim, J. W. (2008). Mutational spectrum of FAM83H: The C-terminal portion is required for tooth enamel calcification. *Human Mutation*, *29*(8), E95–99. https://doi.org/10.1002/humu.20789

Lee, S. K., Lee, K. E., Jeong, T. S., Hwang, Y. H., Kim, S., Hu, J. C., & Kim, J. W. (2011). FAM83H mutations cause ADHCAI and alter intracellular protein localization. *Journal of Dental Research*, *90*(3), 377–381. https://doi.org/10.1177/0022034510389177

Mendoza, G., Pemberton, T. J., Lee, K., Scarel-Caminaga, R., Mehrian-Shai, R., Gonzalez-Quevedo, C., Ninis, V., Hartiala, J., Allayee, H., Snead, M. L., Leal, S. M., Line, S. R. P., & Patel, P. I. (2007). A new locus for autosomal dominant amelogenesis imperfecta on chromosome 8q24.3. *Human Genetics*, *120*(5), 653–662. https://doi.org/10.1007/s00439-006-0246-6

Nitayavardhana, I., Theerapanon, T., Srichomthong, C., Piwluang, S., Wichadakul, D., Porntaveetus, T., & Shotelersuk, V. (2020). Four novel mutations of FAM20A in amelogenesis imperfecta type IG and review of literature for its genotype and phenotype spectra. *Molecular Genetics and Genomics*, *295*(4), 923–931. https://doi.org/10.1007/s00438-020-01668-8

Nowwarote, N., Osathanon, T., Kanjana, K., Theerapanon, T., Porntaveetus, T., & Shotelersuk, V. (2019). Decreased osteogenic activity and mineralization of alveolar bone cells from a patient with amelogenesis imperfecta and FAM83H 1261G>T mutation. *Genes & Diseases*, *6*(4), 391–397. https://doi.org/10.1016/j.gendis.2019.07.005

Nowwarote, N., Theerapanon, T., Osathanon, T., Pavasant, P., Porntaveetus, T., & Shotelersuk, V. (2018). Amelogenesis imperfecta: A novel FAM83H mutation and characteristics of periodontal ligament cells. *Oral Diseases*, *24*(8), 1522–1531. https://doi.org/10.1111/odi.12926

Porntaveetus, T., Abid, M. F., Theerapanon, T., Srichomthong, C., Ohazama, A., Kawasaki, K., & Shotelersuk, V. (2018). Expanding the oro-dental and mutational spectra of kabuki syndrome and expression of KMT2D and KDM6A in human tooth germs. *International Journal of Biological Sciences*, *14*(4), 381–389. https://doi.org/10.7150/ijbs.23517

Pourhashemi, S. J., Ghandehari Motlagh, M., Meighani, G., Ebrahimi Takaloo, A., Mansouri, M., Mohandes, F., & Heidari, M. (2014). Missense mutation in Fam83H gene in Iranian patients with amelogenesis imperfecta. *Iranian Journal of Public Health*, *43*(12), 1680–1687.

Richards, S., Aziz, N., Bale, S., Bick, D., Das, S., Gastier-Foster, J., Grody, W. W., Hegde, M., Lyon, E., Spector, E., Voelkerding, K., & Rehm, H. L. (2015). Standards and guidelines for the interpretation of sequence variants: A joint consensus recommendation of the American College of Medical Genetics and Genomics and the Association for Molecular Pathology. *Genetics in Medicine*, *17*(5), 405–423. https://doi.org/10.1038/gim.2015.30

Smith, C. E. L., Poulter, J. A., Antanaviciute, A., Kirkham, J., Brookes, S. J., Inglehearn, C. F., & Mighell, A. J. (2017). Amelogenesis imperfecta; genes, proteins, and pathways. *Frontiers in Physiology*, *8*, 435. https://doi.org/10.3389/fphys.2017.00435

Song, Y. L., Wang, C. N., Zhang, C. Z., Yang, K., & Bian, Z. (2012). Molecular characterization of amelogenesis imperfecta in Chinese patients. *Cells Tissues Organs*, *196*(3), 271–279. https://doi.org/10.1159/000334210

Thesleff, I. (2003). Epithelial-mesenchymal signalling regulating tooth morphogenesis. *Journal of Cell Science*, *116*(9), 1647–1648. https://doi.org/10.1242/jcs.00410

Urzúa, B., Martínez, C., Ortega-Pinto, A., Adorno, D., Morales-Bozo, I., Riadi, G., Jara, L., Plaza, A., Lefimil, C., Lozano, C., & Reyes, M. (2015). Novel missense mutation of the FAM83H gene causes retention of amelogenin and a mild clinical phenotype of hypocalcified enamel. *Archives of Oral Biology*, *60*(9), 1356–1367. https://doi.org/10.1016/j.archoralbio.2015.06.016

Wang, S. K., Hu, Y., Smith, C. E., Yang, J., Zeng, C., Kim, J. W., & Simmer, J. P. (2019). The enamel phenotype in homozygous Fam83h truncation mice. *Molecular Genetics & Genomic Medicine*, *7*(6), e724. https://doi.org/10.1002/mgg3.724

Wang, S. K., Zhang, H., Hu, C. Y., Liu, J. F., Chadha, S., Kim, J. W., & Hu, J. C. C. (2020). FAM83H and autosomal dominant hypocalcified amelogenesis imperfecta. *Journal of Dental Research*, 22034520962731. https://doi.org/10.1177/0022034520962731

Witkop, C. J., Jr. (1988). Amelogenesis imperfecta, dentinogenesis imperfecta and dentin dysplasia revisited: Problems in classification. *Journal of Oral Pathology*, *17*(9–10), 547–553. https://doi.org/10.1111/j.1600-0714.1988.tb01332.x

Wright, J. T., Frazier-Bowers, S., Simmons, D., Alexander, K., Crawford, P., Han, S. T., & Hart, T. C. (2009). Phenotypic variation in FAM83H-associated amelogenesis imperfecta. *Journal of Dental Reserach*, *88*(4), 356–360. https://doi.org/10.1177/0022034509333822

Wright, J. T., Torain, M., Long, K., Seow, K., Crawford, P., Aldred, M. J., Hart, P. S., & Hart, T. C. (2011). Amelogenesis imperfecta: Genotype-phenotype studies in 71 families. *Cells Tissues Organs*, *194*(2–4), 279–283. https://doi.org/10.1159/000324339

Xin, W., Wenjun, W., Man, Q., & Yuming, Z. (2017). Novel FAM83H mutations in patients with amelogenesis imperfecta. *Scientific Reports*, *7*(1), 6075. https://doi.org/10.1038/s41598-017-05208-0

Yeetong, P., Pongpanich, M., Srichomthong, C., Assawapitaksakul, A., Shotelersuk, V., Tantirukdham, N., Chunharas, C., Suphapeetiporn, K., & Shotelersuk, V. (2019). TTTCA repeat insertions in an intron of YEATS2 in benign adult familial myoclonic epilepsy type 4. *Brain*, *142*(11), 3360–3366. https://doi.org/10.1093/brain/awz267

Yu, S., Quan, J., Wang, X., Sun, X., Zhang, X., Liu, Y., Zhang, C., & Zheng, S. (2018). A novel FAM83H mutation in one Chinese family with autosomal-dominant hypocalcification amelogenesis imperfecta. *Mutagenesis*, *33*(4), 333–340. https://doi.org/10.1093/mutage/gey019

Zhang, C., Song, Y., & Bian, Z. (2015). Ultrastructural analysis of the teeth affected by amelogenesis imperfecta resulting from FAM83H mutations and review of the literature. *Oral Surgery, Oral Medicine, Oral Pathology, and Oral Radiology*, *119*(2), e69–76. https://doi.org/10.1016/j.oooo.2014.09.002

Zheng, Y., Lu, T., Chen, J., Li, M., Xiong, J., He, F., Gan, Z., Guo, Y., Zhang, L., & Xiong, F. U. (2020). The gain-of-function FAM83H mutation caused hypocalcification amelogenesis imperfecta in a Chinese family. *Clinical Oral Investigations*. https://doi.org/10.1007/s00784-020-03609-6

SUPPORTING INFORMATION

Additional supporting information may be found online in the Supporting Information section.

How to cite this article: Sriwattanapong K, Nitayavardhana I, Theerapanon T, et al. Age-related dental phenotypes and tooth characteristics of *FAM83H*-associated hypocalcified amelogenesis imperfecta. *Oral Dis*. 2021;00:1–11. https://doi.org/10.1111/odi.13780